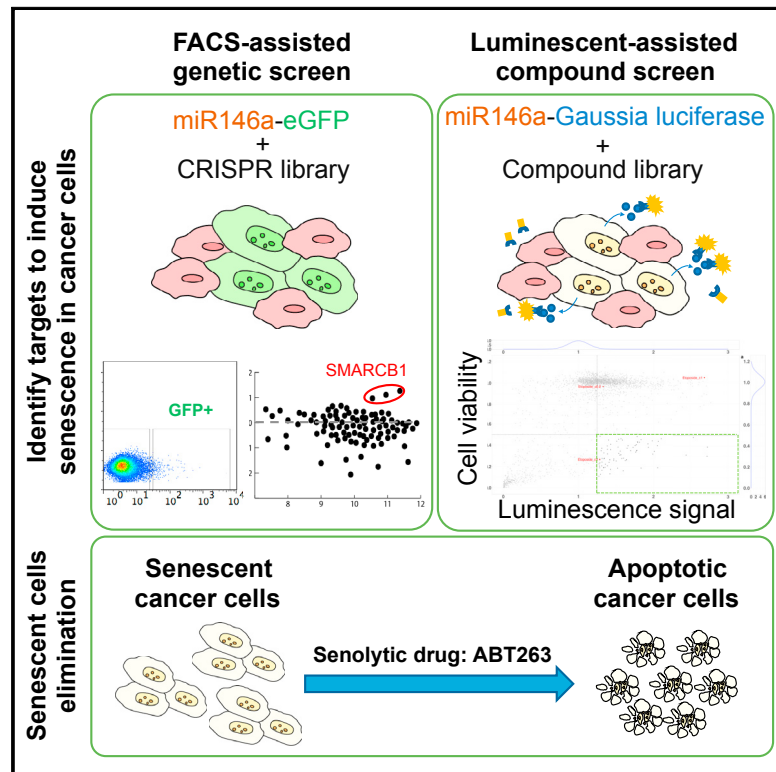


High-Throughput Functional Genetic and Compound Screens Identify Targets for Senescence Induction in Cancer

Graphical Abstract



Authors

Liqin Wang, Rodrigo Leite de Oliveira, Cun Wang, ..., Lisa Willemse, Roderick L. Beijersbergen, René Bernards

Correspondence

r.bernards@nki.nl

In Brief

Wang et al. find that CRISPR-mediated genetic screens and chemical screens serve as two types of high-throughput methods to identify senescence inducers in cancer cells. They also show that senescent cancer cells can be killed selectively by the BCL2-family inhibitor ABT263, providing a potential sequential drug treatment strategy for cancer.

Highlights

- CRISPR and chemical screens identify senescence inducers in cancer cells
- SMARCB1 knockout induces senescence in melanoma
- Aurora kinase inhibition induces senescence in multiple cancer types
- Senescent cancer cells become vulnerable to killing by ABT263

Data and Software Availability

GSE102639



High-Throughput Functional Genetic and Compound Screens Identify Targets for Senescence Induction in Cancer

Liqin Wang,¹ Rodrigo Leite de Oliveira,¹ Cun Wang,¹ João M. Fernandes Neto,¹ Sara Mainardi,¹ Bastiaan Evers,¹ Cor Liefink,¹ Ben Morris,¹ Fleur Jochems,¹ Lisa Willemsen,¹ Roderick L. Beijersbergen,¹ and René Bernards^{1,2,*}

¹Division of Molecular Carcinogenesis, Cancer Genomics Centre, Netherlands Cancer Institute, Plesmanlaan 121, 1066 CX Amsterdam, the Netherlands

²Lead Contact

*Correspondence: r.bernards@nki.nl

<https://doi.org/10.1016/j.celrep.2017.09.085>

SUMMARY

Senescence is a proliferation arrest that can result from a variety of stresses. Cancer cells can also undergo senescence, but the stresses that provoke cancer cells to undergo senescence are unclear. Here, we use both functional genetic and compound screens in cancer cells harboring a reporter that is activated during senescence to find targets that induce senescence. We show that suppression of the SWI/SNF component SMARCB1 induces senescence in melanoma through strong activation of the MAP kinase pathway. From the compound screen, we identified multiple aurora kinase inhibitors as potent inducers of senescence in *RAS* mutant lung cancer. Senescent melanoma and lung cancer cells acquire sensitivity to the *BCL2* family inhibitor ABT263. We propose a one-two punch approach for the treatment of cancer in which a drug is first used to induce senescence in cancer cells and a second drug is then used to kill senescent cancer cells.

INTRODUCTION

Senescence was originally identified through the limited ability of primary fibroblasts in culture to undergo cell division. After the replicative potential of primary cells is exhausted due to telomere shortening, they enter into a stable state of growth arrest termed replicative or cellular senescence (Hayflick, 1965). Senescent cells remain viable, but their cellular state is quite distinct and characterized by absence of proliferation markers, expression of tumor suppressor genes, senescence-associated β -galactosidase (SA- β -gal) activity, and the presence of nuclear foci, referred to as senescence-associated heterochromatin foci (SAHFs) (Muñoz-Espín and Serrano, 2014). Senescent cells also secrete a variety of inflammatory cytokines and chemokines, collectively referred to as the senescence-associated secretory phenotype (SASP), which may help in their clearance from the body (Coppé et al., 2008; Kuilman et al., 2008). With respect to cancer, senescence is generally considered to be a fail-safe mechanism against oncogenic transformation, as

expression of an oncogenic *RAS* gene in primary cells leads to the rapid induction of a post-replicative state referred to as oncogene-induced senescence (OIS) (Serrano et al., 1997). This fail-safe mechanism actually operates in humans to prevent cancer, as melanocytic nevi (moles) often carry an activated *BRAF(V600E)* oncogene, but stain for many of the senescence markers, indicative of a stable and lasting state of oncogene-induced senescence in these cells (Michaloglou et al., 2005). Importantly, even some advanced cancer cells can be induced to enter a state of senescence, not only as a result of chemotherapy treatment but also by excessive oncogenic signaling (Ewald et al., 2010; Sun et al., 2014).

The complex mixture of cytokines, chemokines, growth factors, proteases, and metabolites (collectively called the SASP) produced by senescent cells represents a potentially double-edged sword with respect to tumor control (Coppé et al., 2008, 2010). On the one hand, the SASP can inhibit growth of a cancer by triggering an immunological response against the tumor through recruitment of phagocytic cells and lymphocytes from the adaptive immune system (Eggert et al., 2016). On the other hand, the SASP can also be potentially deleterious. When senescent cells remain present in a tumor, they can contribute to a chronic inflammatory response, which can result in acceleration of age-associated conditions (Baker et al., 2016) and cancer metastases (Angelini et al., 2013). An *in vivo* study showed that elimination of chemotherapy-induced senescent cells reduced several side effects of treatment, including heart toxicity, bone marrow suppression, loss of strength and physical activity, and cancer recurrence and metastasis (Demaria et al., 2017). These latter data indicate that elimination of the senescent cancer cells can be beneficial, while the former data suggest that the SASP may help in immune clearance of cancer cells. The debate whether senescent cancer cells should be eliminated is still ongoing and might ultimately depend on the specific nature of the SASP, as not all senescent cells secrete the same cytokines and chemokines (Hoare et al., 2016).

Senescent cells are quite distinct in terms of gene expression (Fridman and Tainsky, 2008), chromatin structure (Narita et al., 2003), and metabolism (Jiang et al., 2013; Wiley and Campisi, 2016), suggesting that they might be sensitive to certain drugs that do not kill their proliferating counterparts. Indeed, ABT263, a specific inhibitor of the anti-apoptotic proteins *BCL-2*, *BCL-W*, and *BCL-XL*, has been shown to selectively kill

senescent cells *in vivo* in a mouse model to delay several age-associated hematopoietic disorders (Chang et al., 2016; Zhu et al., 2016). This begs the question whether such so called senolytic agents can also be used in a “one-two punch” consecutive therapy approach for cancer in which a first drug is used to induce senescence selectively in cancer cells and a subsequent senolytic therapy serves to eradicate the senescent cancer cells.

Here, we begin to investigate the feasibility of this one-two punch cancer treatment model by performing functional genomic and compound screens to find ways to induce senescence in cancer cells. We show that CRISPR/Cas9-based genetic screens and high-throughput compound screens in cancer cells can be used to identify targets for senescence-inducing therapies. We show that such senescent cancer cells are subsequently sensitive to senolytic agents.

RESULTS

A Reporter-Based CRISPR Screen for Senescence-Inducing Genes

Kang et al. (2015) recently demonstrated that human primary fibroblasts strongly upregulate the expression of microRNA 146a (miR146a) during the process of senescence, irrespective of how senescence was induced. They also demonstrated that a reporter construct in which the promoter of miR146a was linked to EGFP was activated during induction of senescence. We asked whether this miR146a-EGFP reporter was also suited to detect induction of senescence in human cancer cells. We inserted the reporter gene in A375 melanoma cells and induced senescence through treatment with chemotherapy or induction of high levels of reactive oxygen species (ROS). Figures 1A and 1E show that both treatment of the miR146a-EGFP reporter-containing cells with doxorubicin or the ROS-inducer paraquat resulted in a significant upregulation of the EGFP signal, which was associated with the induction of a senescent cell morphology and senescence-associated β -galactosidase (SA- β -gal) activity (Figures 1B, 1C, 1F, and 1G), loss of phosphorylated retinoblastoma protein (p-RB), and the induction of the tumor suppressor protein CDKN1A (also known as p21^{Cip1}) (Figures 1D and 1H).

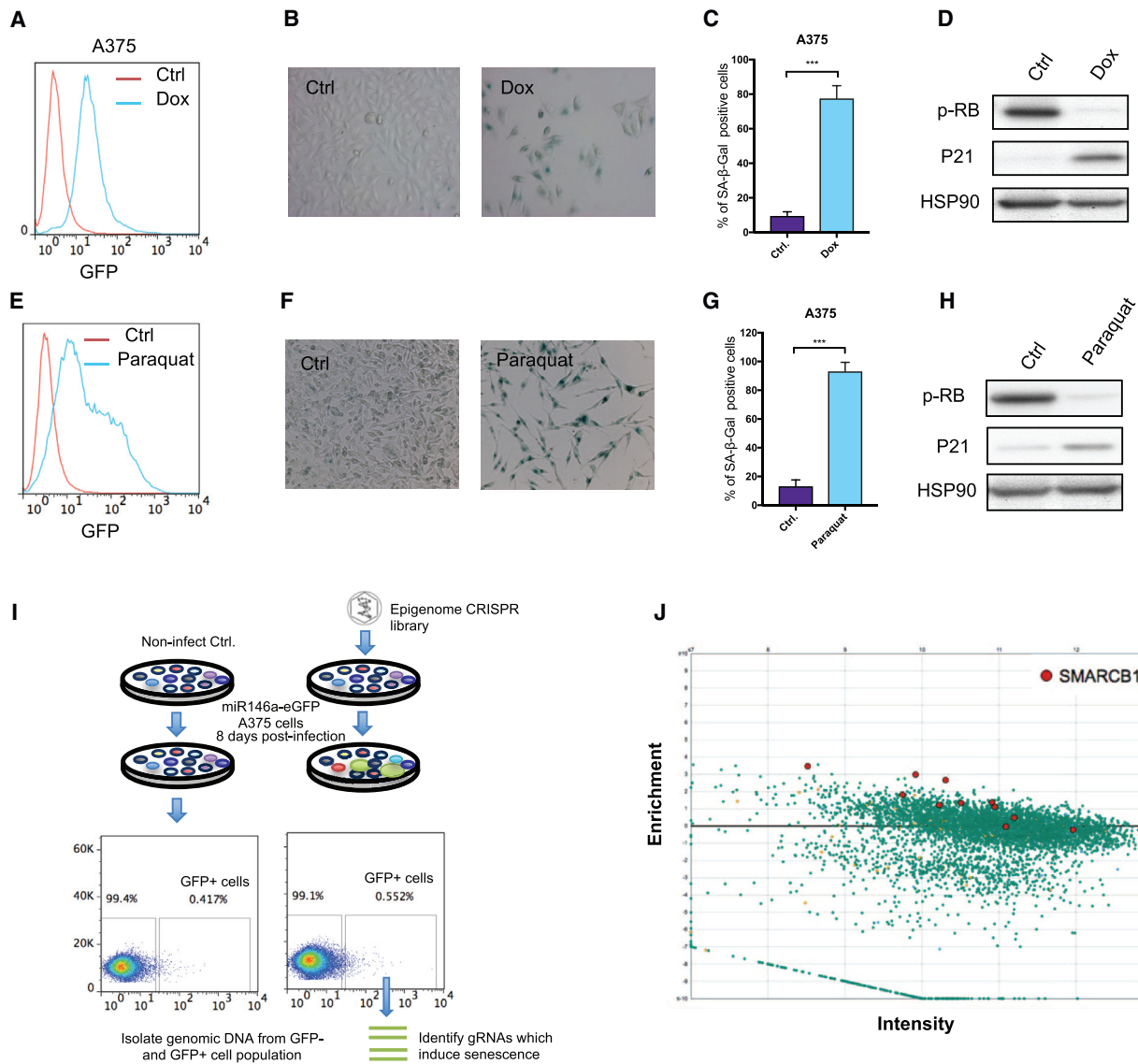
We used these miR146a-EGFP A375 cells for a loss of function genetic screen using a library of 5130 CRISPR vectors targeting 446 enzymes involved in chromatin remodeling and modulation of epigenetic marks (the “epigenome” CRISPR library) (Table S1), as outlined schematically in Figures 1I and 1J. The rationale for the screen is that cells should become EGFP-positive upon the knockout of a gene that induces senescence. After 8 days of culturing, cells were harvested and subjected to fluorescence-activated cell sorting (FACS) into EGFP[−] and EGFP⁺ fractions. Cells without epigenome library served as a control. After this, guide RNA (gRNA) sequences from EGFP[−] and EGFP⁺ cells were recovered by PCR and quantified through deep sequencing as described (Figure 1I) (Evers et al., 2016). A list of significantly enriched gRNAs is provided in Table S1. This list was used for the robust rank algorithm as part of the MAGeCK software, identifying SMARCB1, a component of the SWI/SNF chromatin remodeler complex as top candidate from the screen.

SMARCB1 Knockout Induces Senescence

Because loss of function mutations in SMARCB1 are seen in a range of tumors, including rhabdoid tumors, brain tumors, soft tissue sarcoma, kidney cancer, and Wilms tumor (Hodges et al., 2016), we focused on this gene for further validation. Figures 2A and 2B shows that infection of both A375 and Mel888 melanoma cells with two independent gRNAs targeting SMARCB1 resulted in a dramatic inhibition of proliferation, associated with reduced p-RB and increase in p21^{Cip1} and p27^{Kip1}, both known to be associated with the senescent phenotype. Cells harboring the SMARCB1 gRNAs also had clear signs of senescence as judged by cell morphology and SA- β -gal staining (Figures 2B–2D). Transcriptome analysis of cells infected with gRNAs targeting SMARCB1 revealed that a senescence-associated signature was significantly enriched in these cells (Figure 2G; Table S2). To investigate whether SMARCB1 depletion may also result in cell death, we incubated SMARCB1 knockout cells with caspase-3/7-green fluorescent apoptosis assay reagent, which couples the activated caspase-3/7 recognition motif to a DNA intercalating dye. This enables the quantification of apoptosis. The result shows that SMARCB1 depletion can slightly induce apoptosis in A375 and Mel888 melanoma cells (Figures 2E and 2F). Similar results were seen in two additional melanoma cell lines: Mel526 and Mel624 (Figures S1A–S1E). Note that shortly after infection with SMARCB1, gRNA protein levels were significantly repressed, whereas after 30 days of culturing, the SMARCB1 knockout cells were counter-selected, consistent with an anti-proliferative effect of SMARCB1 loss (Figures S1F–S1H). This is consistent with the notion that a reduction in SMARCB1 levels is associated with a non-proliferative phenotype. Moreover, in miR146a-EGFP A375 cells infected with SMARCB1 gRNA, stronger EGFP positivity was correlated with a stronger anti-proliferative effect and a more pronounced senescence phenotype (Figures 2H and 2I). Similar results were obtained when we used small hairpin RNAs (shRNAs) targeting SMARCB1 instead of gRNAs: three distinct shRNAs against SMARCB1 suppressed SMARCB1 (Figure 2L), induced miR146a-EGFP in two melanoma cell line models (Figure 2K), resulted in suppressed proliferation (Figure 2J), and were associated with a senescent (SA- β -gal positive) morphology (Figures 2M and 2N).

SMARCB1 Activates EGFR through Reduced SOX10 Expression

To gain insight into how SMARCB1 knockout induces senescence, we performed transcriptome analysis using RNA sequencing (RNA-seq). We observed that SOX10 was downregulated upon SMARCB1 depletion (Table S2). We have shown previously that SOX10 suppression can cause resistance to BRAF inhibitors in BRAF mutant melanoma through upregulation of epidermal growth factor receptor (EGFR) through activation of JUN (Sun et al., 2014). Indeed, western blot analyses of cells infected with SMARCB1 gRNAs showed reduced SOX10 protein, which was again associated with an increase in JUN and EGFR mRNA and protein levels (Figures 3A and 3B). Upregulation of EGFR was also associated with increased signaling through the MAP kinase pathway, as evidenced by the increase in p-MEK and p-p90^{RSK}, resulting in hypo-phosphorylation of RB

**Figure 1. The miR-146a-EGFP Reporter Detects Senescence in Melanoma**

(A–D) A375 cells expressing the miR-146-EGFP reporter were treated with 100 ng/mL doxorubicin (DOX) for 120 hr. (A) EGFP fluorescence was measured by flow cytometry. Doxorubicin treatment also induced classic senescence markers: (B) senescence-associated β -galactosidase activity (data were represented as mean \pm SD) and (D) loss of phosphorylated-RB and induction of CDKN1A ($p21^{cip1}$). (C) Quantification of data shown in (B).

(E–H) A375 cells expressing the miR-146-EGFP reporter were treated with 100 μ M paraquat (a ROS inducer) for 120 hr.

(E) EGFP fluorescence was measured by flow cytometry. Doxorubicin treatment also induced classic senescence markers.

(F) Senescence-associated β -galactosidase activity. Data are represented as mean \pm SD.

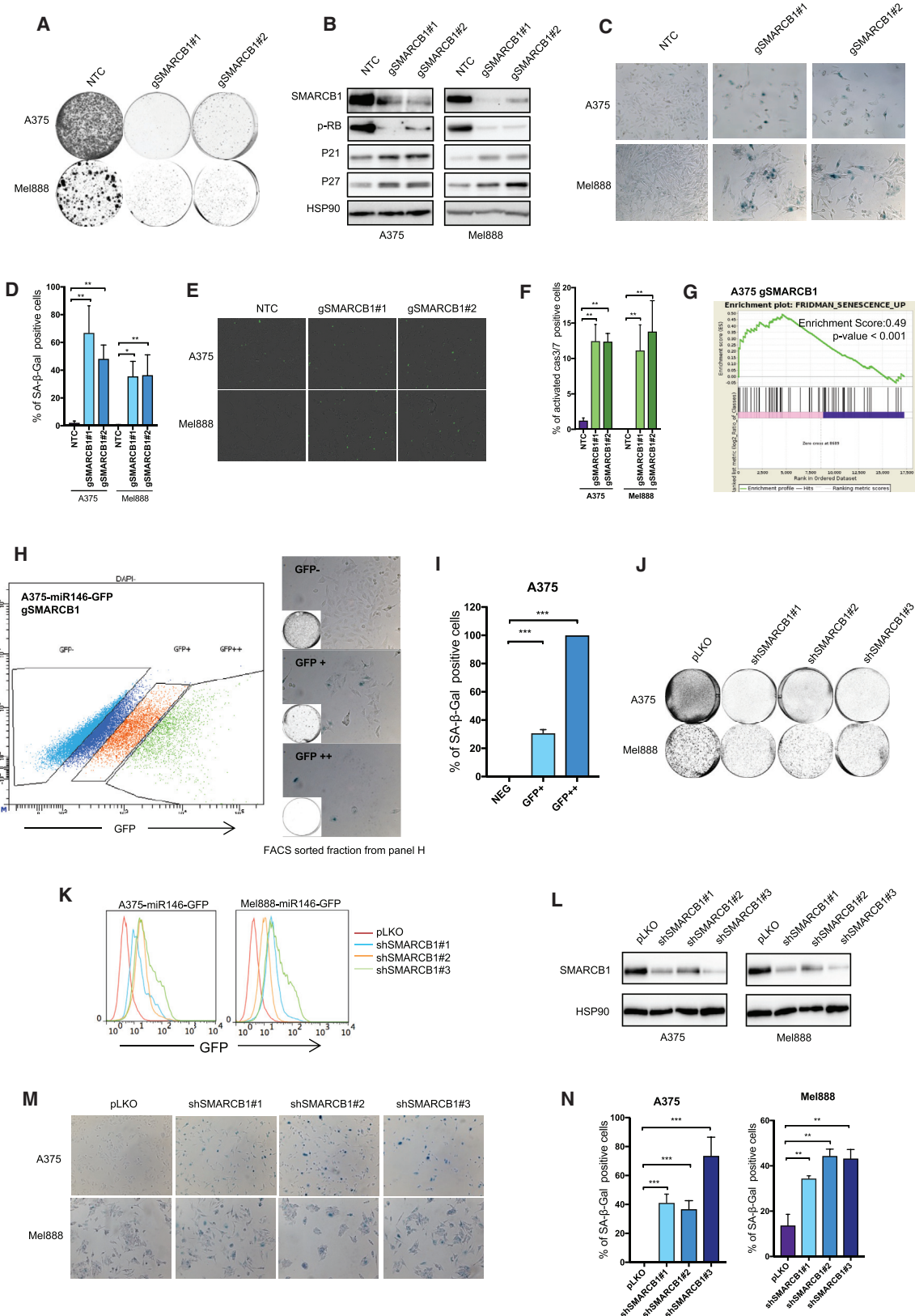
(G) Quantification of data shown in (F). (H) Loss of p-RB and induction of CDKN1A ($p21^{cip1}$).

(I) Schematic outline of the FACS-assisted CRISPR screen. Polyclonal human “epigenome” CRISPR library virus was generated to infect senescence reporter embedded A375-miR146-EGFP cells. These cells were then cultured and collected after 8 days. The collected cells were sorted by fluorescence-activated cell sorter (FACS) into EGFP[−] and EGFP⁺ fractions. The cells without epigenome library viral infection served as a negative control. Subsequently, gRNA inserts from EGFP[−] and EGFP⁺ cell fractions were recovered by PCR and quantified by deep-sequencing.

(J) Representation of the relative abundance of gRNA barcode sequences from the CRISPR screen described in (I). The y axis shows relative abundance (\log_2 value) of gRNA in EGFP⁺ cell fraction versus EGFP[−] cell fraction, and the x axis shows the average number of sequence reads for each gRNA. Positions of the gRNAs targeting SMARCB1 are indicated in red.

and P27^{Kip1} induction (Figure 3A). These data suggested that SMARCB1 knockout could trigger a state that has hallmarks of oncogene-induced senescence, reminiscent of what is seen by

ectopic EGFR expression in melanoma (Sun et al., 2014). Indeed, like EGFR expression, SMARCB1 knockout or shRNA-mediated suppression caused resistance to vemurafenib in A375 cells



(legend on next page)

(Figures 3F and 3G). To ask whether SOX10 suppression is causal in the induction of senescence, we ectopically expressed SOX10 in SMARCB1 knockout cells. Figure 3C shows that SOX10 expression rescues the anti-proliferative effect of SMARCB1 knockout. Biochemically, SOX10 expression down-regulates EGFR expression in the presence of low levels of SMARCB1 and causes reversal of the induction of p27^{kip1}, restoration of RB phosphorylation (Figure 3D), and reduction of SA- β -gal activity (Figure 3E). Conversely, knockdown of SOX10 by shRNA vector activated the miR146a-EGFP vector, consistent with a state of oncogene-induced senescence (Figures S2A and S2B).

The specific inhibitor of the anti-apoptotic proteins BCL-2, BCL-W, BCL-XL, and ABT263 (navitoclax), selectively kills senescent cells, but no data are published on senescent cancer cells (Chang et al., 2016; Zhu et al., 2016). We therefore tested whether senescence induced by SMARCB1 downregulation in melanoma cells made them vulnerable to ABT263. Figures 3H–3J show that ABT263 had little effect on parental A375 cells, but effectively ablated cells harboring a gRNA targeting SMARCB1. Figures 3K and 3L show that ABT263 can massively induce apoptosis in melanoma cells made senescent through SMARCB1 depletion. Similar results were obtained in Mel624 cells (Figures S2C and S2D). Together, these data demonstrate the feasibility of killing cancer cells with a sequential therapy in which a vulnerability is acquired by a first drug that is targeted by a second drug.

Compound Screens for Senescence Induction

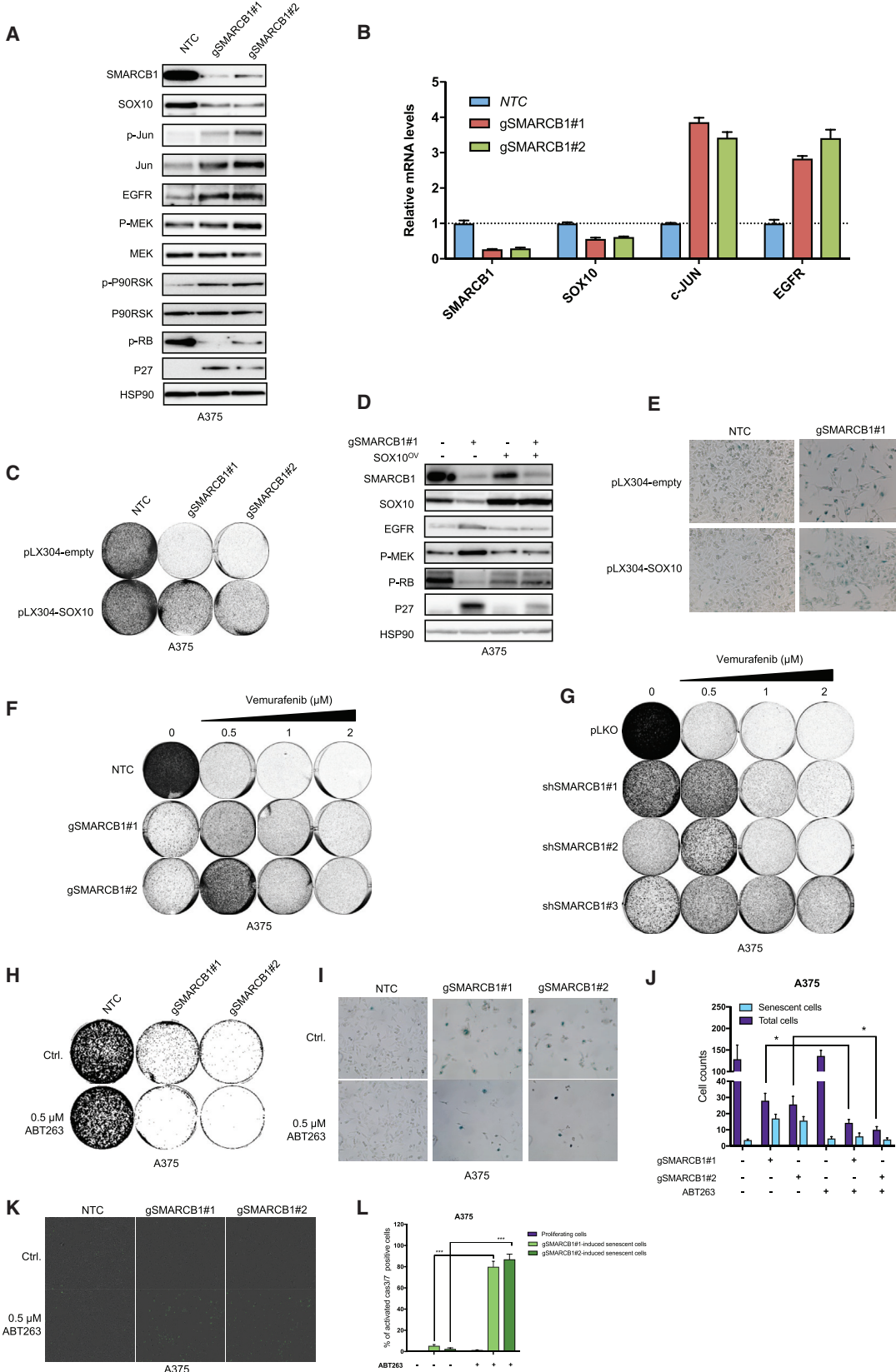
To screen for compounds that induce senescence in RAS mutant lung cancer, we reconfigured the miR146a-EGFP vector to express the secreted *Gaussia luciferase* (Gluc) under control of the miR146a promoter. KRAS mutant A549 lung cancer cells were stably transfected with the miR146a-Gluc reporter and then seeded into 384 well plates. After 24 hr, cells were incubated with 0.2, 1, and 5 μ M of 941 unique compounds from 4 independent libraries, including inhibitors of G protein-coupled receptors, a library targeting kinases, an epigenetic modifying enzyme library, and an NCI-approved oncology drug set. After 7 days, senescence induc-

tion was assessed by the luminescence signal, quantified with an Envision plate reader, while the cell viability was determined by a CellTiter-Blue assay (Figure 4A). The chemotherapeutic agent etoposide was included in the screen as a positive control. Figures S3A–S3E show that etoposide indeed efficiently induces senescence in both A549 and H358 lung cancer cells.

Figure 4B shows the normalized values of CellTiter-Blue (ctb) and Gaussia luciferase (luc) per compound. There are two major categories of hits in the screen: those with high luciferase in the presence of high CellTiter-Blue and relatively high luciferase with low CellTiter-Blue. This may be explained by a rapid versus a slow onset of a senescence response following compound addition (Figure 4B; Table S3). Among the 47 top outliers are 18 independent aurora kinase inhibitors as strong inducers of the reporter construct (Figure 4C; Table S4). Indeed, treatment of A549 KRAS mutant lung cancer cells with aurora kinase inhibitors induced a marked senescence response, as judged by morphology and SA- β -gal expression (Figures 4D and 4E), induction of p21^{cip1} and hypo-phosphorylated RB (Figure 4F), enrichment of senescence-associated gene signature (Figure 4G; Table S2), and reduction of proliferation (Figure 4H). Notably, aurora kinase inhibition initially induced apoptosis. However, apoptosis rate was significantly reduced once the cells started to show the flat senescence-associated morphology (Figures 4I, 4J, S4H, and S4I). Similar results were obtained in p53 null H358 KRAS mutant lung cancer cells (Figures S4A–S4F), indicating that aurora kinase inhibitor-induced senescence is p53-independent. Additionally, aurora kinase inhibitor alisertib also induced senescence in several other cancer models, including RAS mutant melanoma (SK-MEL-2), colorectal cancers (HCT116 and SW1463), a pancreatic cancer cell line (Panc1), a triple negative breast cancer (Cal51), and two liver cancer lines (Huh7 and Hep3B) (Figures S4J and S4K). Moreover, when aurora kinase inhibitors were used to induce senescence in A549 or H358 lung cancer cells, they became sensitive to the senolytic agent ABT263 (Figures 4K–4P and S4G). Similar results were obtained with etoposide (Figures S3F–S3I). ABT199, which inhibits only BCL2 and not BCL-XL, did not eliminate the senescent A549 cells (Figures S3J and S3K), indicating

Figure 2. SMARCB1 Depletion Induces Senescence in Melanoma Cells

- (A–D) A375 and Mel888 cells expressing the miR146a-EGFP reporter were infected with two independent SMARCB1 gRNAs-CAS9 (gSMARCB1) virus and cultured for 10 days. (A) Depletion of SMARCB1 reduced cell proliferation and upregulated classic senescence markers. (B) Loss of p-RB, induction of CDKN1A (p21^{cip1}) (C), CDKN1B (27^{kip1}) (D), and increased senescence-associated β -galactosidase activity (quantification shown in D, data were represented as mean \pm SD). Non-targeted gRNA vector (NTC) served as a control.
- (E) A375 cells were infected with two independent SMARCB1 gRNAs-CAS9 (gSMARCB1) virus and cultured for 5 days. Afterward, the cells were seeded in 96-well plates and incubated with caspase-3/7 green apoptosis assay reagent. Images were taken by IncuCyte after 4 days. Green fluorescent staining indicated caspase-3/7-dependent apoptosis (quantification shown in F, data were represented as mean \pm SD).
- (F) As in (E), for Mel888 melanoma cells.
- (G) A375 cells were infected with gRNAs gSMARCB1 virus and cultured for 8 days, RNA sequencing was performed on these cells, and followed by GSEA analysis for the “FRIDMAN_SENESCENCE_UP” geneset: A375 cells infected with gSMARCB1-1 versus A375 cells infected with a non-targeting control gRNA (see the *Supplemental Experimental Procedures*). The Enrichment Score was 0.49 with a p value of <0.001.
- (H and I) A375 cells expressing the miR146a-EGFP reporter were infected with SMARCB1 gRNA virus and cultured for 8 days, (H) subsequently FACS sorted into GFP[−], GFP⁺, and GFP⁺⁺ cell fraction. The sorted cells were seeded 20,000 in a 6-well plate, cultured for additional 7 days, followed by senescence β -galactosidase staining. Quantification shown in (I). Data were represented as mean \pm SD.
- (J) A375 and Mel888 cells expressing the miR146a-EGFP reporter were infected with three independent shRNAs targeting SMARCB1 (shSMARCB1). Empty vector pLKO served as a control.
- (K) GFP levels of miR146-eGFP expressing cells infected with shRNAs-targeting SMARCB1, (L) western blot showing suppressed SMARCB1 expression after shRNA SMARCB1 infection (M) staining for senescence-associated β -galactosidase activity of cells infected with shRNA SMARCB1 (N), quantification of data shown in (M). Data were represented as mean \pm SD.



(legend on next page)

a critical role for BCL-like factors in killing senescent cancer cells (Souers et al., 2013). Together, these data indicate that both functional genetic screens and compound screens using miR146a reporter assays can identify targets and compounds that induce senescence in cancer cells.

DISCUSSION

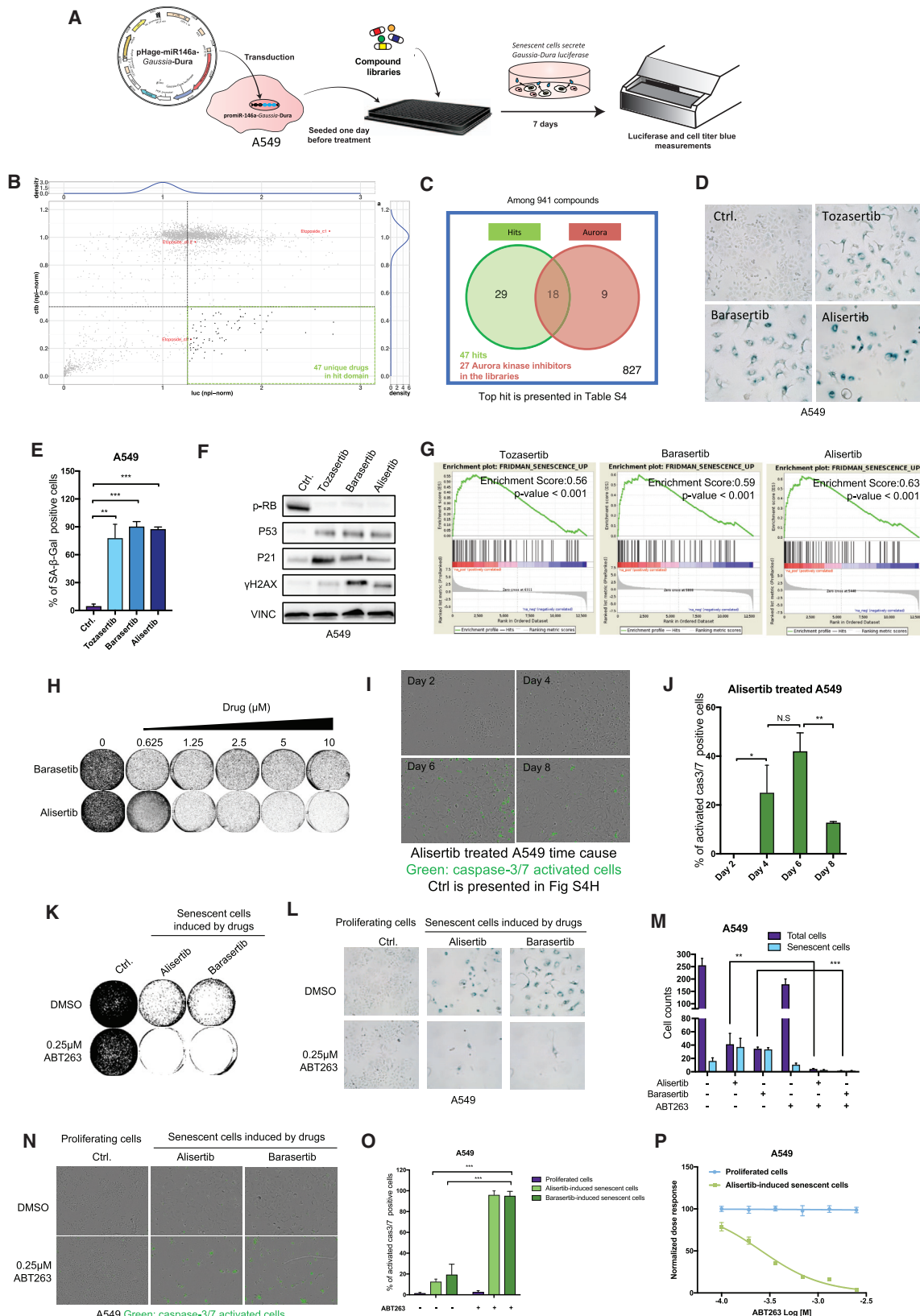
Drug resistance is the biggest obstacle to the effective treatment of cancer. When patients fail first line treatment, they are often offered second and even third line therapies in the hope to provoke a response with a drug that is mechanistically distinct from the first line therapy. In general, such subsequent therapies are less effective than first line therapy. To address these issues, we explore the induction of senescence as a potential anti-cancer strategy. Although speculative, senescence-inducing therapies may help ameliorate drug resistance in two different ways. First, drug resistance is often the result of the selective outgrowth of a pre-existing sub-population of drug-resistant cells in the tumor. Senescence is known to induce a strong inflammatory response through the secreted SASP and such tumor-infiltrating inflammatory cells may help killing the subset of non-senescent cells through a bystander effect. In this context, it is interesting to note that treatment of *BRAF* mutant melanoma is almost invariably associated with resistance after 6–8 months, whereas CTLA-4 mediated immune cell activation for the same cancers leads to far longer-lasting effects (Flaherty et al., 2010; Schadendorf et al., 2015). A priori, there is no reason to believe that there are pre-existing variants conferring resistance to *BRAF* inhibitor treatment (explaining the rapid resistance development), but that mutations that confer resistance to CTLA-4 therapy are not pre-existent in the tumor. A possible explanation for this discrepancy is that immune infiltrates can kill sub-fractions of unresponsive tumor cells through a bystander effect. If correct, such bystander effect may also help prevent resistance to senescence-inducing therapies.

Induction of a senescence-like phenotype has been described as a side effect of a number of cancer drugs (Ewald et al., 2010). The difference with the approach used here is that through high-throughput screens, we aim to identify the most potent senescence-inducing agents. Such strong pro-senescence agents may be more powerful than the therapy-induced senescence described in the literature. It will be important to address in future experiments, which fraction of a cancer cell population must be made senescent to eradicate the tumor completely. This will help elucidate to which extent a bystander effect is helping in clearing subsets of non-senescent cancer cells.

A second way in which senescence-inducing cancer therapies could help in fighting drug resistance relates to the fact that second line therapies are often less effective than first line therapy. Senescent cells are very different from their proliferating counterparts in terms of gene expression, chromatin state, and metabolism, which suggests that killing them with selective agents should be feasible (Fridman and Tainsky, 2008; Narita et al., 2003; Wiley and Campisi, 2016). Indeed, a first generation of senolytic agents has been described to kill senescent cells, but such compounds were not tested extensively on senescent cancer cells to date. We show here that ABT263, but not the related ABT199, can kill a range of senescent cancer cells, independent of how senescence was induced. Based on our findings, we propose a “one-two punch” approach to the treatment of cancer. In the first treatment of the cancer, senescence is induced selectively in the cancer, which is exploited in a consecutive therapy that kills senescent cells. The attractive aspect of a sequential treatment strategy is that the second therapy takes advantage of a major vulnerability induced by the first therapy. For this reason, a second therapy could be very effective in this scenario. A further attractive thought, albeit highly speculative at present, is that senolytic agents have been shown to increase lifespan in mice due to the delay of age-related pathologies (Baar et al., 2017; Baker et al., 2016). Thus, a senolytic agent used in the

Figure 3. SMARCB1 Depletion Induces Oncogene-Induced Senescence through Downregulation of SOX10

- (A and B) A375 cells expressing the miR146a-EGFP reporter were infected with two independent gSMARCB1 and cultured for 10 days.
- (A) Western blot analysis shows that depletion of SMARCB1 results in a reduction of SOX10, induction of JUN, phosphorylated-JUN (p-JUN), EGFR, and hyper-activated MAP kinase signaling as judged by phosphorylated-MEK (p-MEK), phosphorylated-P90^{RSK} (p-P90RSK), phosphorylated-RB (p-RB), and P27^{Kip}. HSP90 served as a loading control.
- (B) Real-time PCR showing relative mRNA level of SOX10, JUN, and EGFR upon *SMARCB1* depletion. Data were represented as mean ± SD.
- (C–E) A375 cells were infected with SOX10 overexpressing lentiviral vector and selected with blasticidin. Subsequently, cells were infected with gRNAs-CAS9 targeting SMARCB1 and selected with puromycin.
- (C) Colony formation assay demonstrating that depletion of SMARCB1 reduced cell proliferation, but this can be rescued by overexpressing SOX10.
- (D) Protein level of SMARCB1, SOX10, EGFR, p-MEK, p-RB, and p27 were measured by western blot. HSP90 served as a loading control.
- (E) SOX10 overexpressing partially reduced the SA-β-gal activity that was induced by SMARCB1 depletion.
- (F) Depletion of SMARCB1 using gRNAs-CAS9 confers a proliferation disadvantage in the absence of the BRAF-inhibitor vemurafenib, but induces vemurafenib resistance in A375 cells. After 5 days post-infection of gSMARCB1-CAS9, the cells were seeded 50,000 per well in 6-well plates and cultured for 12 days in the presence or absence of vemurafenib.
- (G) A375 cells were infected with shRNAs targeting SMARCB1, seeded 50,000 per well in 6-well plates, and cultured in the presence or absence of vemurafenib for 10 days.
- (H–J) A375 cells were infected with SMARCB1 gRNAs-CAS9 virus. 4 days post-infection, the cells were seeded into 6-well plates and treated with 0.5 μM ABT263 for 120 hr.
- (H) Colony formation assay showed that ABT263 selectively depleted cells, which were infected with SMARCB1 gRNAs-CAS9.
- (I) Cells with increased senescence-associated β-galactosidase activity are vulnerable to ABT263.
- (J) Quantification of data shown in (K). Data were represented as mean ± SD.
- (K) A375 infected with two independent SMARCB1 gRNAs-CAS9 (gSMARCB1) virus and cultured for 8 days. Then, the cells were seeded in 96-well plates, treated with 0.5 μM ABT263, and incubated with caspase-3/7 green apoptosis assay reagent. Images were taken by IncuCyte after 72 hr. Green fluorescent staining indicated caspase-3/7-dependent apoptosis.
- (L) Quantification of data shown in (K). Data were represented as mean ± SD.



(legend on next page)

treatment of cancer could contribute to patient rejuvenation, a significant departure from the side effects caused by current cancer therapies. How senescence-inducing and senolytic agents should be administered (sequential, overlapping, concurrent) will require extensive testing in immunocompetent animal models and may also depend on the nature of the SASP produced by the cancer cells.

Here, we show that large-scale functional genomic screens can be used to identify drug targets that would be useful in achieving a senescent state in cancer cells. There are a number of important questions that must still be addressed. Which are the most effective triggers to induce senescence in cancer cells? Are these senescence triggers similar or distinct in cancers originating from different tissues? Are there commonalities in the senescence triggers in relation to their genotype? Having high-throughput screening systems in place to find these senescence triggers, we should be able to address these questions in the near future.

EXPERIMENTAL PROCEDURES

Further details and an outline of resources used in this work can be found in the [Supplemental Experimental Procedures](#).

Cell Lines

The A375, SK-Mel-2 melanoma cell lines, H358 and A549 lung cancer cell lines, HCT116, SW1463 colon cancer cell lines, and Panc1 pancreatic cancer

cell line were obtained from ATCC. Mel888, Mel624, and Mel526 cells were gifts from D. Peepoer (Amsterdam, the Netherlands). Cal51 breast cancer line was obtained from K. Jastrzebski (NKI, Amsterdam, the Netherlands). Huh7 and Hep3B liver cancer cell lines were obtained from S. Huang (NKI, Amsterdam, the Netherlands). A375, Mel888, Mel624, Mel526, Huh7, Hep3B, and SK-Mel-2 were cultured in a DMEM-based medium supplemented with 10% FBS, 1% penicillin/streptomycin, and 2 mM L-glutamine. Cal51 were cultured in a DMEM-based medium supplemented with 20% FBS, 1% penicillin/streptomycin, and 2 mM L-glutamine. HCT116, SK1463, Panc1, A549, and H358 were cultured in a RPMI-based medium supplemented with 10% FBS, 1% penicillin/streptomycin, and 2 mM L-glutamine. All the cell lines have been validated by STR profiling and regularly tested for Mycoplasma spp with PCR-based assay.

FACS-Assisted Genetic Screen with a Customized CRISPR Epigenetic Library

Lentiviral CRISPR V2.1 (LC2.1) encoding gRNAs that target epigenetic genes are listed in [Table S1](#). Lentiviral supernatants of the plasmids were produced as described at <https://www.broadinstitute.org/rnai/public/resources/protocols>.

A375-miR146-GFP cells were infected with 3 independent biological replicates. Cells were then seeded at 350,000 cells per 15-cm dish, and the medium was refreshed every 3 days for 8 days. Non-infected A375-miR146-GFP cells were taken as the control. Then, the cells were collected and suspended in D-MEN medium containing 2% FCS. BD FACSAria III (BD Bioscience) was used to sort out GFP⁺ cells. The FACS data were analyzed by FlowJo program version 7.6.5 (Tree Star). The genomic DNA was isolated from GFP⁻ and GFP⁺ cells using DNasey Blood and Tissue Kit (#69506 QIAGEN). gRNA inserts were recovered from DNA by PCR amplification, PCR product purification was performed using High Pure PCR Product

Figure 4. A Compound Screen Identifies Aurora Kinase Inhibitors as Inducers of Senescence

- (A) Schematic outline of compound screen. The miR146-GFP reporter was modified to express Gaussia luciferase. The reporter was introduced into a KRAS mutant lung cancer line A549 through lentiviral infection. The infected cells were seeded into 384-well plates. After 24 hr, the compound library containing 941 unique pharmacologically active compounds was added into the plates. Three concentrations were used: 0.2 μM, 1 μM, and 5 μM in 3 biological replicates. After 7 days, the Gaussia luminescence signal was measured with 5 μg/mL coelenterazine, and cell viability signal was measured with 25 times diluted CellTiter-Blue with Envision Multilabel Plate Reader.
- (B) Results from the compound screen. The NPI normalized (npi-norm) values for CellTiter-Blue signal (ctb) and luminescent signal (luc) were plotted for each compound. The hits were defined based on the selection criteria that: (1) the value for the luciferase readout should be ≥ 1.25 and corresponds with a p value of 0.032, and (2) the value of the CellTiter-Blue readout should be ≤ 0.5 and corresponds with a p value of 4.1e-14. The p values were calculated based on the null-distributions formed by the negative control (DMSO). Etoposide served as a positive control. The top hits were presented in the hit domain.
- (C) Among 941 unique compounds in the combined drug library, there were 27 unique aurora kinase inhibitors. 47 compounds were considered as hits. Among these 47 drug hits, 18 were independent aurora kinase inhibitors.
- (D–H) A549 cells were treated with 0.2 μM tozasertib, 1 μM alisertib, or 1 μM barasertib for 7 days.
- (D) Treatment with three independent aurora kinase inhibitors induced senescence-associated β-galactosidase activity (quantification shown in E, data were represented as mean ± SD).
- (E) Quantification of data shown in (D).
- (F) Aurora kinase inhibitor treatment also induced classic senescence markers: loss of phosphorylated-RB, upregulation of P53, and CDKN1A (p21^{Cip1}). Induction of γH2AX was also observed. VINC served as a loading control.
- (G) RNA sequencing was performed on these cells, and followed by GSEA analysis of tozasertib-, barasertib-, or alisertib-treated cells versus untreated control for the “FRIDMAN_SENESCENCE_UP” geneset.
- (H) Aurora kinase inhibitors treatment also reduced proliferation in A549.
- (I) A549 cells were seeded in 96-well plates, treated with 0.5 μM alisertib, and incubated with caspase-3/7 green apoptosis assay reagent. Images were taken by IncuCyte at different time points. Green fluorescent staining indicated caspase-3/7-dependent apoptosis.
- (J) Quantification is shown in (I).
- (K–M) The aurora kinase inhibitors-induced senescent A549 cells were seeded into 6-well plates and treated with ABT263. Parental A549 were used as a control.
- (K) Colony formation assay demonstrated that aurora inhibitors-induced senescent cells were selectively sensitive to ABT263 compared to proliferating cells.
- (L) Alisertib pre-treated cells stained strongly positive for senescence-associated β-galactosidase activity, and these cells can be significantly depleted with ABT263 within 96 hr.
- (M) The quantification of remaining cells and senescent cells is shown. Data were represented as mean ± SD.
- (N and O) The aurora kinase inhibitors-induced senescent A549 cells were seeded into 96-well plates, treated with ABT263, and incubated with caspase-3/7 green apoptosis assay reagent.
- (N) Images were taken by IncuCyte at 48 hr. Green fluorescent staining indicated for caspase-3/7-dependent apoptosis.
- (O) Quantification is shown. Data were represented as mean ± SD.
- (P) The aurora kinase inhibitors-induced senescent A549 cells were seeded into 96-well plates with three biological replications and treated with a different dose of ABT263 for 72 hr. Drug-dose response was determined based on CellTiter-Blue measurement. Data were represented as mean ± SD.

Purification Kit according to manufacturers' instruction (#11732676001, Roche). Screen result analysis details are described in [Evers et al. \(2016\)](#).

PCR, Next-Generation Sequencing, and Data Analysis

Each sample is divided over PCR reactions containing 500 ng DNA, with a maximum of 20 µg DNA to cover the complexity. Barcoded PCR primers were used for the first PCR reaction. Each PCR reaction consisted of 500 ng DNA, 10 µL GC buffer (5×), 1 µL forward primer (10 µM), 1 µL reverse primer (10 µM), 1 µL dNTPs (10 mM), 1.5 µL DMSO, and 0.5 µL polymerase in a total volume of 50 µL. PCR program consisted of initial denaturation at 98°C for 2 min, 16 cycles of 30 s denaturation at 98°C, 30 s of annealing at 60°C, and 30 s elongation at 72°C, with a final extension at 72°C for 5 min. PCR products of each sample were pooled, and 2.5 µL was used for a second PCR reaction in technical duplicates. Primers in this reaction contained barcodes and an adaptor sequence for next-generation sequencing. PCR mixtures and program were the same as for the first PCR. PCR products of the second PCR were purified with a DNA purification kit (28-9034-70; GE Healthcare.). Sample concentrations were measured with BioAnalyzer and were pooled equimolarly. Inserted gRNA sequences were identified by Illumina HiSeq 2500 genome analyzer at the Genomics Core Facility (NKI). The mapped read counts were normalized using DESeq2 and used as input for the alpha Robust Rank Algorithm of MAGeCK software version 0.5.

Drug Screen with Compound Libraries

Using the Multidrop Combi (Thermo Scientific), 200 A549 cells expressing miR-146a-Gaussia-Dura-luciferase were seeded in 60 µL into 384-well plates. After 24 hr, the combined compound libraries of inhibitor including G protein-coupled receptors, kinase, epigenetic modifying enzymes, and NCI-approved oncology drug set were added. This library was stored and handled as recommended by the manufacturer. Compounds from the master plate were diluted in daughter plates containing complete RMPI medium, using the MICROLAB STAR liquid handling workstation (Hamilton). From the daughter plates, 15 µL of the diluted compounds was transferred into 384-well assay plates, in triplicate, with final concentrations of 0.2 µM, 1 µM, and 5 µM. After 7 days, the protein levels of Gaussia-Dura luciferase were determined by a luciferase assay as described in [Degeling et al. \(2013\)](#). Five minutes before measurement, 10 µL Coelenterazine diluted to 5 µg/mL was added. The luminescence signal was measured with the Envision Multilabel Plate Reader (PerkinElmer) at 400–700 nm. After this, a CellTiter-Blue assay was performed (G8081/2; Promega) as recommended by the manufacturer. Both the fluorescent and CTB data were normalized per plate using the normalized percentage inhibition (NPI) method. NPI sets the mean of the positive control value to 0 and mean of the negative control to 1. Per compound and concentration, the mean was determined over the three replicates for both the CellTiter-Blue readout and for the Luciferase readout. A null distribution of the negative controls was created, and the mean value of the biological replicates was tested for significance. Etoposide was considered as a positive control in the screen.

CRISPR Epigenome Library Generation

For the design of the CRISPR library, 5,130 gRNAs were selected targeting 446 genes involved in epigenetic processes. gRNAs were designed such that when possible, 10 gRNAs target each transcript associated with the gene in the first 50% of the ORF. Further selection involved maximizing sequence divergence from potential off-target sites and optimizing the library size by choosing gRNAs that were shared between transcripts targeting the same gene. In addition, 50 gRNAs targeting 10 essential genes and 50 non-targeting gRNAs were added to the design. Oligo's with gRNA sequences flanked by adapters were ordered from CustomArray (Bothell, WA) and cloned as a pool by GIBSON assembly in LentiCRISPRv2.1 ([Evers et al., 2016](#)).

qRT-PCR

Total RNA was extracted from cells using TRIzol reagent from Invitrogen or Quick-RNA MiniPrep (#R1055) from Zymo Research. cDNA synthesis was performed using Maxima Universal First Strand cDNA Synthesis Kit (#K1661) from Thermo Scientific. qPCR reactions were performed with FastStart Universal SYBR Green Master (Rox) from Roche. The experiments were performed according to the manufacturer's instructions. The sequences of the primers

used for qRT-PCR analyses are described in the [Supplemental Experimental Procedures](#). All reactions were run in triplicate. The computed tomography (CT) values were calculated using the standard curve method.

CRISPR gRNA Generation

Oligonucleotides containing gRNA sequences ([Supplemental Experimental Procedures](#)) flanked by 20–30 nt of overlapping backbone sequence were obtained from ThermoFisher scientific gRNA sequences were cloned into Len-tiCRISPRv2.1 via *Bsm*BI sites, using Gateway cloning strategy.

Lentiviral Transduction

A third-generation lentivirus packaging system consisting of pCMV-VSV-G (Addgene #8454), pRSV-Rev (Addgene #12253), and pMDLG/pRRE (Addgene #12251) was used to create virus particles of the modified reporter plasmids. A transient transfection was performed in 293T cells and lentiviral supernatants were produced. Destination cells were infected with lentiviral supernatants, using 8 µg/mL Polybrene and low virus titer. After 48 hr of incubation, the supernatant was replaced by medium containing 10 µg/mL BSD or 2 µg/mL puromycin. After 48 hr, selection of viral transduced cell lines was completed.

Long-Term Cell Proliferation Assays

Cells were seeded into 6-well plates and cultured both in the absence and presence of drugs as indicated. The cells were then cultured for indicated time (in figure legends). At the end of assay, the cells were fixed with 4% PFA, stained with crystal violet, and photographed.

Staining for β-Galactosidase Activity

β-galactosidase activity in cells was detected using Histochemical Staining Kit (CS0030-1KT) from Sigma-Aldrich. β-galactosidase detection was carried out according to the manufacturer's instructions. SA-beta-gal staining positive cells were quantified based on 3 independent images from different regions of the stainings.

IncuCyte Caspase-3/7 Green Apoptosis Assay

Cells were seeded in 96-well plate. After 24 hr, IncuCyte Caspase-3/7 Green Apoptosis Assay Reagent (#4440) from Essen Bioscience was added with 1,000 times dilution to each well. Experiments were performed with 3 independent biological triplicates. The pictures were taken using IncuCyte. Caspase-3/7-activated cells were quantified based on 3 images generated from independent biological replicates.

Protein Lysate Preparation and Immunoblots

Cells lysates were collected followed by washing with PBS and lysing with RIPA buffer supplemented with protease inhibitor (cComplete, Roche) and Phosphatase Inhibitor Cocktails II and III (Sigma). All lysates were freshly prepared and processed with Novex NuPAGE® Gel Electrophoresis Systems (Invitrogen).

Flow Cytometry

Cells were harvested and suspended in 300 µL medium. GFP-positivity was determined with excitation at 486 nm, at the CyAn ADP flow cytometer (DakoCytomation). The mean value of GFP fluorescent signal was determined with FlowJo version 7.6.5. GraphPad prism version 7.0 was used for data analysis.

Statistical Analysis

Throughout all figures: * $p \leq 0.05$, ** $p \leq 0.01$, and *** $p \leq 0.001$ and N.S. (not significant) $p > 0.05$. Statistical t test analyses were performed using Microsoft Excel or PRISM.

DATA AND SOFTWARE AVAILABILITY

The accession number for the raw and processed data from the next generation RNA sequencing to profile senescence gene signature upon SMARCB1-knockout on A375, etoposide-, tozasertib-, barasertib-, and alisertib-treated A549 reported in this paper is NCBI Gene Expression Omnibus (GEO): GSE102639.

SUPPLEMENTAL INFORMATION

Supplemental Information includes Supplemental Experimental Procedures, four figures, and four tables and can be found with this article online at <https://doi.org/10.1016/j.celrep.2017.09.085>.

AUTHOR CONTRIBUTIONS

L.W. co-designed the study, performed experiments, and wrote the manuscript. R.B. co-designed the study and supervised the project. All authors contributed to the experiments and commented on the manuscript text.

ACKNOWLEDGMENTS

We thank Stephen Elledge for the kind gift of the miR-146a-EGFP vector. This work was funded by a grant from the Dutch Cancer Society (KWF) and the Center for Cancer Genomics (CGC).

Received: May 26, 2017

Revised: August 29, 2017

Accepted: September 25, 2017

Published: October 17, 2017

REFERENCES

- Angelini, P.D., Zacarias Fluck, M.F., Pedersen, K., Parra-Palau, J.L., Guiu, M., Bernadó Morales, C., Vicario, R., Luque-García, A., Navalpotro, N.P., Giralt, J., et al. (2013). Constitutive HER2 signaling promotes breast cancer metastasis through cellular senescence. *Cancer Res.* 73, 450–458.
- Baar, M.P., Brandt, R.M.C., Putavet, D.A., Klein, J.D.D., Derk, K.W.J., Bourgeois, B.R.M., Stryeck, S., Rijken, Y., van Willigenburg, H., Feijtel, D.A., et al. (2017). Targeted apoptosis of senescent cells restores tissue homeostasis in response to chemotoxicity and aging. *Cell* 169, 132–147.
- Baker, D.J., Childs, B.G., Durik, M., Wijers, M.E., Sieben, C.J., Zhong, J., Saltiness, R.A., Jeganathan, K.B., Verzosa, G.C., Pezeshki, A., et al. (2016). Naturally occurring p16(INK4a)-positive cells shorten healthy lifespan. *Nature* 530, 184–189.
- Chang, J., Wang, Y., Shao, L., Laberge, R.M., Demaria, M., Campisi, J., Janakiraman, K., Sharpless, N.E., Ding, S., Feng, W., et al. (2016). Clearance of senescent cells by ABT263 rejuvenates aged hematopoietic stem cells in mice. *Nat. Med.* 22, 78–83.
- Coppé, J.P., Patil, C.K., Rodier, F., Sun, Y., Muñoz, D.P., Goldstein, J., Nelson, P.S., Desprez, P.Y., and Campisi, J. (2008). Senescence-associated secretory phenotypes reveal cell-nonautonomous functions of oncogenic RAS and the p53 tumor suppressor. *PLoS Biol.* 6, 2853–2868.
- Coppé, J.P., Desprez, P.Y., Krtolica, A., and Campisi, J. (2010). The senescence-associated secretory phenotype: the dark side of tumor suppression. *Annu. Rev. Pathol.* 5, 99–118.
- Degeling, M.H., Bovenberg, M.S., Lewandrowski, G.K., de Gooijer, M.C., Vleugel-Lankamp, C.L., Tannous, M., Maguire, C.A., and Tannous, B.A. (2013). Directed molecular evolution reveals *Gaussia luciferase* variants with enhanced light output stability. *Anal. Chem.* 85, 3006–3012.
- Demaria, M., O'Leary, M.N., Chang, J., Shao, L., Liu, S., Alimirah, F., Koenig, K., Le, C., Mitin, N., Deal, A.M., et al. (2017). Cellular senescence promotes adverse effects of chemotherapy and cancer relapse. *Cancer Discov.* 7, 165–176.
- Eggert, T., Wolter, K., Ji, J., Ma, C., Yevsa, T., Klotz, S., Medina-Echeverz, J., Longerich, T., Forques, M., Reisinger, F., et al. (2016). Distinct functions of senescence-associated immune responses in liver tumor surveillance and tumor progression. *Cancer Cell* 30, 533–547.
- Evers, B., Jastrzebski, K., Heijmans, J.P., Grernrum, W., Beijersbergen, R.L., and Bernards, R. (2016). CRISPR knockout screening outperforms shRNA and CRISPRi in identifying essential genes. *Nat. Biotechnol.* 34, 631–633.
- Ewald, J.A., Desotelle, J.A., Wilding, G., and Jarrard, D.F. (2010). Therapy-induced senescence in cancer. *J. Natl. Cancer Inst.* 102, 1536–1546.
- Flaherty, K.T., Puzanov, I., Kim, K.B., Ribas, A., McArthur, G.A., Sosman, J.A., O'Dwyer, P.J., Lee, R.J., Grippo, J.F., Nolop, K., and Chapman, P.B. (2010). Inhibition of mutated, activated BRAF in metastatic melanoma. *N. Engl. J. Med.* 363, 809–819.
- Fridman, A.L., and Tainsky, M.A. (2008). Critical pathways in cellular senescence and immortalization revealed by gene expression profiling. *Oncogene* 27, 5975–5987.
- Hayflick, L. (1965). The limited in vitro lifetime of human diploid cell strains. *Exp. Cell Res.* 37, 614–636.
- Hoare, M., Ito, Y., Kang, T.-W., Weekes, M.P., Matheson, N.J., Patten, D.A., Shetty, S., Parry, A.J., Menon, S., Salama, R., et al. (2016). NOTCH1 mediates a switch between two distinct secretomes during senescence. *Nat. Cell Biol.* 18, 979–992.
- Hodges, C., Kirkland, J.G., and Crabtree, G.R. (2016). The many roles of BAF (mSWI/SNF) and PBAF complexes in cancer. *Cold Spring Harb. Perspect. Med.* 6, a026930.
- Jiang, P., Du, W., Mancuso, A., Wellen, K.E., and Yang, X. (2013). Reciprocal regulation of p53 and malic enzymes modulates metabolism and senescence. *Nature* 493, 689–693.
- Kang, C., Xu, Q., Martin, T.D., Li, M.Z., Demaria, M., Aron, L., Lu, T., Yankner, B.A., Campisi, J., and Elledge, S.J. (2015). The DNA damage response induces inflammation and senescence by inhibiting autophagy of GATA4. *Science* 349, aaa5612.
- Kuilman, T., Michaloglou, C., Vredeveld, L.C., Douma, S., van Doorn, R., Desmet, C.J., Aarden, L.A., Mooi, W.J., and Peepoer, D.S. (2008). Oncogene-induced senescence relayed by an interleukin-dependent inflammatory network. *Cell* 133, 1019–1031.
- Michaloglou, C., Vredeveld, L.C., Soengas, M.S., Denoyelle, C., Kuilman, T., van der Horst, C.M., Majoor, D.M., Shay, J.W., Mooi, W.J., and Peepoer, D.S. (2005). BRAF600-associated senescence-like cell cycle arrest of human naevi. *Nature* 436, 720–724.
- Muñoz-Espín, D., and Serrano, M. (2014). Cellular senescence: from physiology to pathology. *Nat. Rev. Mol. Cell Biol.* 15, 482–496.
- Narita, M., Nuñez, S., Heard, E., Narita, M., Lin, A.W., Hearn, S.A., Spector, D.L., Hannon, G.J., and Lowe, S.W. (2003). Rb-mediated heterochromatin formation and silencing of E2F target genes during cellular senescence. *Cell* 113, 703–716.
- Schadendorf, D., Hodi, F.S., Robert, C., Weber, J.S., Margolin, K., Hamid, O., Patt, D., Chen, T.T., Berman, D.M., and Wolchok, J.D. (2015). Pooled analysis of long-term survival data from phase ii and phase iii trials of ipilimumab in unresectable or metastatic melanoma. *J. Clin. Oncol.* 33, 1889–1894.
- Serrano, M., Lin, A.W., McCurrach, M.E., Beach, D., and Lowe, S.W. (1997). Oncogenic ras provokes premature cell senescence associated with accumulation of p53 and p16INK4a. *Cell* 88, 593–602.
- Souers, A.J., Leverson, J.D., Boghaert, E.R., Ackler, S.L., Catron, N.D., Chen, J., Dayton, B.D., Ding, H., Enschede, S.H., Fairbrother, W.J., et al. (2013). ABT-199, a potent and selective BCL-2 inhibitor, achieves antitumor activity while sparing platelets. *Nat. Med.* 19, 202–208.
- Sun, C., Wang, L., Huang, S., Heynen, G.J.J.E., Prahalad, A., Robert, C., Haanen, J., Blark, C., Wesseling, J., Willem, S.M., et al. (2014). Reversible and adaptive resistance to BRAF(V600E) inhibition in melanoma. *Nature* 508, 118–122.
- Wiley, C.D., and Campisi, J. (2016). From ancient pathways to aging cells-connecting metabolism and cellular senescence. *Cell Metab.* 23, 1013–1021.
- Zhu, Y., Tchkonia, T., Fuhrmann-Stroissnigg, H., Dai, H.M., Ling, Y.Y., Stout, M.B., Pirtskhalava, T., Giorgadze, N., Johnson, K.O., Giles, C.B., et al. (2016). Identification of a novel senolytic agent, navitoclax, targeting the Bcl-2 family of anti-apoptotic factors. *Aging Cell* 15, 428–435.